Title

Mesoscopic Constructs of Ordered and Oriented Metal—Organic Frameworks on Plasmonic Silver Nanocrystals

Journal

Journal of the American Chemical Society, 137(6)

ISSN

0002-7863

Authors

Zhao, Yingbo
Kornienko, Nikolay
Liu, Zheng
et al.

Publication Date

2015-02-18

DOI

10.1021/ja512951e

Peer reviewed

Mesoscopic constructs of ordered and oriented metal-organic frameworks on plasmonic silver nanocrystals

Yingbo Zhao,[1†] Nikolay Kornienko,[1†] Zheng Liu,[2] Chenhui Zhu,[3] Shunsuke Asahina,[4] Tsung-Rong Kuo,[1] Wei Bao,[1] Chenlu Xie,[1] Alex Hexemer,[3] Osamu Terasaki,[5,6] Peidong Yang[1]* and Omar M. Yaghi[1,7]*

[1]Department of Chemistry, University of California-Berkeley, Materials Sciences Division, Lawrence Berkeley National Laboratory, Kavli Energy NanoSciences Institute, Berkeley, California 94720, USA.

[2]Nanotube Research Center, AIST, Tsukuba 305-8565, Japan.

[3]Advanced Light Source, Lawrence Berkeley National Lab, Berkeley, California, 94720, USA.

[4]SMBU, JEOL Ltd., Akishima, Tokyo 196-8558, Japan.

[5]Department of Materials and Environmental Chemistry, and EXSELENT, Stockholm University, Stockholm, Sweden.

[6]Graduate School of EEWS, WCU/BK21Plus, KAIST, Daejeon 305-701, Republic of Korea.

[7]King Abdulaziz City of Science and Technology, P.O. Box 6086, Riyadh, Saudi Arabia.

[†]Contributed equally to this work

[*]Correspondence to: p_yang@berkeley.edu and yaghi@berkeley.edu

Abstract

We have enclosed octahedral silver nanocrystals by metal-organic frameworks (MOFs) to make mesoscopic constructs O_h-nano-Ag⊂MOF in which the interface between the silver and the MOF is pristine, the MOF is ordered (crystalline), and oriented on the silver nanocrystals. This unique construct is achieved by atomic layer deposition of aluminum oxide on silver nanocrystals and addition of tetra-topic porphyrin based linker [4,4',4",4'"-(porphyrin-5,10,15,20-tetrayl)tetrabenzoic acid, H_4TCPP] to react with alumina and make MOF [$Al_2(OH)_2$TCPP] enclosures around silver nanocrystals. Alumina thickness is precisely controlled from 0.1 to 3 nm, thus allowing control of the MOF thickness from 10 to 50 nm. Electron microscopy and grazing angle x-ray diffraction confirm the order and orientation of the MOF in this construct by virtue of the porphyrin units being perpendicular to the planes of the silver. The mesoscopic construct provides a unique opportunity to use surface enhanced Raman spectroscopy (SERS) to directly track the metalation process on the porphyrin and map the distribution of the metalated and unmetalated linkers on a single nanoparticle level—aspects yet unrealized in MOFs.

Inorganic nanocrystals are important because they occupy a size regime intermediate between small molecules and extended structures. Their chemistry has been largely explored through surface functionalization. The fundamental problem is that it is difficult to control the spatial arrangement and order of the functional units and therefore the chemistry occurring at the interface between the inorganic nanocrystal and an incoming substrate. We believe that this 'functionalization problem' could be overcome by using metal-organic frameworks (MOFs) as well-defined units for which the spatial arrangement of functional organic and inorganic units, porosity, density and thickness can be precisely controlled. Addressing this problem requires a new synthetic approach to overcome four challenges: (a) a pristine interface between inorganic nanocrystals and MOFs that is free of surfactants and other surface ligands to take advantage of synergistic effects at the interface, (b) well-ordered and precisely oriented MOF enclosures around the inorganic nanocrystals to impart high degree of spatial control over the desired functional groups, (c) sufficiently thin MOF enclosures for facile diffusion and high resolution chemical mapping, and (d) bridging multiple length scales by combining the MOF atomically defined scale with the nano dimension for plasmonic structures, thus realizing new chemical and physical functions. In this way, it would be possible to construct mesoscopic assemblies where the MOF and the plasmonic nanocrystals are linked across multiple length scales yet operate differently and synergistically.

Although efforts to grow MOFs on inorganic nanocrystals have been made, a general method addressing all four challenges has not emerged (*1-14*). In this work, a

general method has been developed to overcome these four challenges using atomic layer deposition (ALD) technique where a thin metal oxide film is deposited onto plasmonic silver nanocrystals and used as a metal ion source to nucleate the desired MOF when the appropriate organic linker is added (Scheme 1). We show that ALD allows control of MOF thickness by controlling the metal oxide thickness, while the slow release of metal ions from the metal oxide layer results in control of crystallinity of MOF and ultimately its orientation on the silver nanocrystals. The MOF crystallinity, orientation, and the pristine interface thus produced enabled metalation and linker variation chemistry to be carried out on the MOF-silver nanocrystal mesoscopic construct. Integration of MOF onto nanocrystal surfaces further enables the direct probing of such chemistry by surface enhanced Raman spectroscopy (SERS) using the plasmonic silver nanocrystal substrates. Specifically, we show that the course of metalation in a porphyrin based MOF can be tracked and, in addition, different chemical signatures within MOF can be imaged at high spatial resolution down to a single nanoparticle level.

On a fundamental level, this system is an illustrative example of how two materials of self-similar structures can be combined into a mesoscopic ensemble of heterogeneous construction yet endowed with precisely defined chemical, spatial and metric characteristics (*15*). This coupled to the demonstrated ability to make mesoscopic constructs of these MOF-inorganic nanocrystals provides an unparalleled opportunity for tracking, probing and mapping of passing molecules; an aspect that is expected to be a boon for catalytic chemical conversions, sensing and imaging

applications.

Our strategy to overcome the functionalization problem involves making silver nanoparticle-MOF constructs (O_h-nano-Ag⊂MOF) in which silver nanoparticles are wrapped by MOF enclosures. Silver octahedra were synthesized by the polyol method: silver nitrate salt is reduced by a pentanediol solvent and polyvinylpyrolidone (PVP) employed as a surfactant (*16*) . Silver nanocrystals are selected as a model plasmonic metal nanostructure as they have intense local surface plasmon resonances in the visible range and have been extensively studied as SERS substrates (*17, 18*) . The chosen MOF is $Al_2(OH)_2$(TCPP) [H_4TCPP: 4,4',4",4"'-(porphyrin-5,10,15,20-tetrayl) tetrabenzoic acid], which consists of chains of corner-sharing aluminum octahedra running along the *b*-axis and connected by the TCPP units through the carboxylate groups (Fig. 1) (*19*) . This MOF was synthesized in bulk by reacting H_4TCPP with $AlCl_3$ in water at 180°C to give large, microcrystalline powder.

With the eventual goal of creating thin films of this MOF on the silver surface, we chose to use ALD thin films as a localized metal precursor source. The fabrication procedure of the O_h-nano-Ag⊂MOF begins with the deposition of Al_2O_3 films on the silver nanocrystals as the aluminum source for the MOF synthesis. The silver nanocrystal is drop cast on a silicon substrate and conformal, thickness-controlled alumina is deposited at 60°C using trimethylaluminum and water as precursor at a deposition rate of 0.1 nm/cycle (fig. S1). The alumina coated silver nanocrystals are converted to MOF by reacting with the TCPP linker. However, the original hydrothermal condition used to synthesize this MOF would not be appropriate as the

high temperature will melt the silver nanocrystals and the TCPP linker is not soluble enough in water to sufficiently react with alumina. Considering this, the reaction temperature was reduced to 140°C, and *N*,*N*-dimethylformamide (DMF) water mixed solvent is used, containing 5 mg H_4TCPP dissolved in 1.5 ml DMF and 0.5 ml H_2O. The conversion of alumina to MOF was carried out in a sealed glass tube in a microwave reactor using, in the initial runs, 20 nm thick layers of alumina. Unfortunately, an interfacial 10 nm thick alumina layer between the MOF and the silver was observed instead of the desired pristine interface. This lead us to reduce the alumina layer thickness to below 3 nm and found it to be sufficient to eliminate the interfacial alumina layer while enabling the fabrication of conformal and thin MOF enclosures (Scheme 1).

We next utilized Raman spectroscopy to characterize the MOF composition of the thin film and in particular detect the signature of the porphyrin building units in the MOF. However, we found that the PVP at the interface between the silver and MOF gave a strong signal which overwhelmed the Raman spectrum. We address this issue by employing an additional surface cleaning step using a Meerwein's salt treatment to remove PVP surfactant before coating the silver with ALD alumina to ensure a pristine interface between the MOF and Ag nanocrystal (fig. S2) (*20*) . Following the surfactant removal, the MOF conversion was carried out again, and only the strong TCPP signal was visible in the Raman spectrum (fig. S3).

The phase purity and high crystallinity of the MOF enclosures synthesized using 1, 5, and 30 cycles of ALD Al_2O_3 is confirmed by grazing incidence wide angle x-ray

scattering (GIWAXS) measurements (fig. S4). Scanning electron microscopy (SEM) was used to characterize the morphology of O_h-nano-Ag⊂MOF, and showed that the shape of the silver nanocrystal is retained throughout the process of fabrication and crystalline plate-like MOF regions are visible on the silver nanocrystal surface (Fig. 2A, B, fig. S5).

We proceeded to quantify the thickness control of the resulting MOF enclosures by controlling the ALD layer thickness. Fig. 2 shows typical SEM and transmission electron microscopy (TEM) images of MOF films obtained from alumina layer thicknesses of 3, 0.5, and 0.1 nm (Fig. 2C to H). With increased cycles of alumina, the size and coverage of MOF crystallites on the Ag surface as well as the overall MOF layer thickness increases. The average thickness of the MOF enclosures are approximately 50 nm, 25 nm, and 10 nm for 30 cycles, 5 cycles, and 1 cycle ALD alumina, respectively (Fig. 2F to H). At the lowest limits of the ALD precursor film thickness of less than one nanometer, highly crystalline MOF enclosures as thin as several nanometers were made (fig. S6). The crystallite size and morphology of the MOF was finely tuned by varying the reaction conditions: a water:DMF ratio of 3:1 solvent mixture results in a more uniform, conformal MOF enclosure in contrast to the plate-like structure (fig. S7).

The MOF crystallinity and orientation at the interface was examined by high resolution TEM. Imaging under the accelerating voltage of 120 kV with a low electron dosage, MOF lattice fringes were observed (Fig. 3A). This confirms, at a microscopic level, the high crystallinity of the MOF enclosure at the interface and the

fact it is pristine. The orientation of the MOF regions was determined from the TEM images (Fig. 3B), where the lattice fringes of 1.6 nm correspond to the MOF (200) planes parallel to the interface. This indicates that the porphyrin units of the MOF are perpendicular to the silver surface. The two dimensional lattice fringes of 1.16 nm, which correspond to MOF (201) plane, are also observed (Fig. 3C), and thus provide an unambiguous determination of the MOF orientation being perpendicular to the silver surface. Detailed analysis of the silver and MOF orientation is described in SI (section S3). No evidence of porphyrin units oriented parallel to the silver surface was found among the TEM images. Energy dispersive x-ray spectroscopy (EDS) elemental mapping was utilized to further confirm the enclosed structure of the O_h-nano-Ag⊂MOF as described further below.

GIWAXS structural analysis is performed on a macroscopic level using a flat silicon substrate for MOF growth to further confirm the crystallinity and orientation of the MOF at an ensemble level. The spot pattern on GIWAXS image (Fig. 3D) matches that expected for the preferred orientation of the MOF with the porphyrin units perpendicular to the substrate (MOF [200] direction perpendicular to the substrate). A random orientation of the MOF would result in a ring rather than a spot pattern in the GIWAXS image. This oriented growth is also observed when glass is used as substrate to grow the MOF (fig. S16), which suggests that the oriented MOF growth is not substrate specific. The TEM and GIWAXS findings combined lead to a structural model of the MOF-substrate interface (Fig. 3E), in which the porphyrin units of the MOF are perpendicular to the interface. This clearly demonstrates that this

synthetic approach is well-suited for fabricating crystalline and precisely oriented MOF enclosures on inorganic nanocrystals. Knowledge of the porphyrin orientation to the silver nanocrystals also conveys their spatial arrangement and allowed us to carry out, for the first time on a nanocrystal substrate, chemistry specific to the porphyrin units (metalation with cobalt, see below) and probe it by SERS.

It is worth noting that this approach for making mesoscopic constructs can also produce MOF on other substrates such as carbon disk with the same morphology and crystallinity (section S4). In addition, this method of MOF fabrication is also applicable to a variety of MOFs made up of other metals. Here, the appropriate metal oxide could be used as a precursor. For example, a film of ALD indium oxide was used as the metal precursor to react with H_4TCPP to give an isoreticular (having the same net topology) indium MOF as the present aluminum MOF (figs. S22, S23). Different linkers could also be used to react with the same oxide to give the corresponding MOF, as in the case of DUT-5 (*21*), in which biphenyl-4,4′-dicarboxylic acid was used (figs. S24, S25). A member of a subclass of MOFs, ZIF-8, could also be fabricated using ALD zinc oxide (figs. S26, S27). We expect that since this MOF fabrication approach is substrate independent, it is generalizable and can be extended to produce multiple oriented and ordered MOF enclosures on a variety of inorganic nanostructures.

With the ability to form thin MOF enclosures on plasmonic nanocrystals without an interfacial surfactant layer, unprecedented opportunities emerge in high resolution probing of chemical processes in MOF using SERS. The pristine interface enables the

synergistic effects between the MOF enclosure and the silver nanocrystals. In a O_h-nano-Ag⊂MOF sample, all peaks in the SERS spectrum match those of the bulk MOF and the TCPP molecule and can be assigned according to previous literature studies of porphyrin molecules (*22, 23*) (fig. S3). This spectroscopic handle allowed us to track the metalation of the porphyrin units within the MOF enclosure. Metalation was carried out by heating the O_h-nano-Ag⊂MOF in a 10 mg/ml cobalt acetate methanol solution at 100°C under microwave irradiation (section S6). The metalation of the porphyrin molecule is evidenced mainly by the decline of the ν_8 mode corresponding to the free base porphyrin at 330 cm^{-1} and the rise of the ν_8 mode of the metalated porphyrin at 390 cm^{-1} (*22*). This is further confirmed by UV-Vis (fig. S28) and energy dispersive x-ray (EDS) spectroscopies where in the latter, elemental mapping is utilized to further confirm the enclosed structure of the O_h-nano-Ag⊂MOF (fig. S29). Within the enclosure of MOF, this post-synthetic metalation is tracked with SERS (Fig. 4A) and found to be complete within 50 minutes; thus pointing to the facile diffusion of the cobalt acetate reagent due to the porosity of the MOF and access to the silver interface.

Confocal SERS mapping is next applied to study heterogeneous MOF enclosures on silver nanocrystals and the unique capability of this system to generate spatially resolved chemical information. The size of an O_h-nano-Ag⊂MOF octahedron is 300 nm, which is similar to the diffraction limited spatial resolution possible with a 532 nm laser in a confocal microscopy setup. Therefore, chemical information at the limit of a single silver nanoparticle can be obtained. The

multivariate approach, in which different organic linkers are incorporated into the same framework, is a powerful technique to introduce heterogeneity and complexity into MOFs and one that has presented challenges to its characterization due to lack of techniques capable of deciphering the spatial arrangement of the linkers (*24, 25*).

Here, pre-metalated porphyrin linker, cobalt (II) 4,4',4",4"'-(porphyrin-5,10,15,20-tetrayl)tetrabenzoic acid, was mixed with the unmetalated TCPP linker in a 1:3 ratio in the precursor solution and reacted with the alumina coated silver nanocrystals under the conditions described above. The SERS spectrum was measured on clusters of O_h-nano-Ag⊂MOF particles, and found to have peaks attributable to ν_8 mode of both the metalated and unmetalated forms of the porphyrin unit. One of the fundamental difficulties in nano-MOF chemistry is to decipher whether the nanoparticles as a whole are homogenous in their composition, especially when a multivariate approach in metalation or mixing of linkers is employed in the synthesis of the MOF. The materials prepared here allow us to address this issue. Mapping of the metalated and unmetalated linkers in a monolayer of O_h-nano-Ag⊂MOF using SERS reveals a well-mixed porphyrin system. In that, on the single particle level there is no segregation of metalated and unmetalated regions of the MOF (Fig. 4C, D). This is quantified by the ratio of the Raman scattering intensity of the two ν_8 modes for the metalated and unmetalated. This ratio is obtained from integrating the corresponding peaks and it is found to lie at 1.5 which is in between all metalated and all unmetalated scenarios (Fig. 4C), which indicates that the distribution is homogenous from particle to particle as evidenced from mapping 7

μm regions (Fig. 4D, section S8).

To illustrate the power of combining MOF and plasmonic nanocrystal into one mesoscopic construct, O_h-nano-Ag⊂MOF, we examined an area occupied by multiple discrete particles for their chemical composition using confocal Raman spectroscopy. Fig. 4F and G shows the area of particles and their corresponding SERS maps, respectively. It is very clear that because of the thin enclosure of MOF around the silver, it is possible to observe strong SERS signals for each of the particles and furthermore within each such particle the metalated and unmetalated porphyrin units in the MOF can be observed. This is possible because the MOF is grown on a plasmonic inorganic nanocrystal with a clean interface. Comparison of Fig. 4F and G also reveals that the SEM and SERS mapping are consistent in providing a highly resolved picture of the spatial arrangement of the mesoscopic O_h-nano-Ag⊂MOF particles.

References and notes

1. L. He *et al.*, Core–Shell Noble-Metal@Metal-Organic-Framework Nanoparticles with Highly Selective Sensing Property. *Angew. Chem. Int. Ed.* **52**, 3741 (2013).
2. P. Hu *et al.*, Surfactant-Directed Atomic to Mesoscale Alignment: Metal Nanocrystals Encased Individually in Single-Crystalline Porous Nanostructures. *J. Am. Chem. Soc.* **136**, 10561 (2014).
3. Y. Hu, J. Liao, D. Wang, G. Li, Fabrication of Gold Nanoparticle-Embedded Metal–Organic Framework for Highly Sensitive Surface-Enhanced Raman Scattering Detection. *Anal. Chem.* **86**, 3955 (2014).
4. S. Jin *et al.*, Energy Transfer from Quantum Dots to Metal–Organic Frameworks for Enhanced Light Harvesting. *J. Am. Chem. Soc.* **135**, 955 (2013).
5. K. Khaletskaya *et al.*, Integration of Porous Coordination Polymers and Gold Nanorods into Core–Shell Mesoscopic Composites toward Light-Induced

Molecular Release. *J. Am. Chem. Soc.* **135**, 10998 (2013).
6. L. E. Kreno *et al.*, SERS of molecules that do not adsorb on Ag surfaces: a metal-organic framework-based functionalization strategy. *Analyst* **139**, 4073 (2014).
7. L. E. Kreno, J. T. Hupp, R. P. Van Duyne, Metal−Organic Framework Thin Film for Enhanced Localized Surface Plasmon Resonance Gas Sensing. *Anal. Chem.* **82**, 8042 (2010).
8. N. Liu *et al.*, Functionalization of silicon nanowire surfaces with metal-organic frameworks. *Nano Res.* **5**, 109 (2012).
9. G. Lu *et al.*, Imparting functionality to a metal–organic framework material by controlled nanoparticle encapsulation. *Nat. Chem.* **4**, 310 (2012).
10. J. Reboul *et al.*, Mesoscopic architectures of porous coordination polymers fabricated by pseudomorphic replication. *Nat. Mater.* **11**, 717 (2012).
11. O. Shekhah *et al.*, Layer-by-Layer Growth of Oriented Metal Organic Polymers on a Functionalized Organic Surface. *Langmuir* **23**, 7440 (2007).
12. M. C. So *et al.*, Layer-by-Layer Fabrication of Oriented Porous Thin Films Based on Porphyrin-Containing Metal–Organic Frameworks. *J. Am. Chem. Soc.* **135**, 15698 (2013).
13. K. Sugikawa, Y. Furukawa, K. Sada, SERS-Active Metal–Organic Frameworks Embedding Gold Nanorods. *Chem. Mater.* **23**, 3132 (2011).
14. W.-w. Zhan *et al.*, Semiconductor@Metal–Organic Framework Core–Shell Heterostructures: A Case of ZnO@ZIF-8 Nanorods with Selective Photoelectrochemical Response. *J. Am. Chem. Soc.* **135**, 1926 (2013).
15. H. Furukawa, K. E. Cordova, M. O'Keeffe, O. M. Yaghi, The Chemistry and Applications of Metal-Organic Frameworks. *Science* **341**, (2013).
16. A. Tao, P. Sinsermsuksakul, P. Yang, Polyhedral Silver Nanocrystals with Distinct Scattering Signatures. *Angew. Chem. Int. Ed.* **45**, 4597 (2006).
17. A. Tao, P. Sinsermsuksakul, P. Yang, Tunable plasmonic lattices of silver nanocrystals. *Nat. Nanotechnol.* **2**, 435 (2007).
18. A. R. Tao *et al.*, Self-Organized Silver Nanoparticles for Three-Dimensional Plasmonic Crystals. *Nano Lett.* **8**, 4033 (2008).
19. A. Fateeva *et al.*, A Water-Stable Porphyrin-Based Metal–Organic Framework Active for Visible-Light Photocatalysis. *Angew. Chem. Int. Ed.* **51**, 7440 (2012).
20. E. L. Rosen *et al.*, Exceptionally Mild Reactive Stripping of Native Ligands from Nanocrystal Surfaces by Using Meerwein's Salt. *Angew. Chem. Int. Ed.* **51**, 684 (2012).
21. I. Senkovska *et al.*, New highly porous aluminium based metal-organic frameworks: Al(OH)(ndc) (ndc = 2,6-naphthalene dicarboxylate) and Al(OH)(bpdc) (bpdc = 4,4′-biphenyl dicarboxylate). *Microporous Mesoporous Mater.* **122**, 93 (2009).
22. B. Vlckova *et al.*, Surface-enhanced resonance Raman spectra of free base 5, 10, 15, 20-tetrakis (4-carboxyphenyl) porphyrin and its silver complex in systems with silver colloid: direct adsorption in comparison to adsorption via

molecular spacer. *J. Phy. Chem.* **97**, 9719 (1993).
23. X. Y. Li *et al.*, Consistent porphyrin force field. 1. Normal-mode analysis for nickel porphine and nickel tetraphenylporphine from resonance Raman and infrared spectra and isotope shifts. *J. Phy. Chem.* **94**, 31 (1990).
24. X. Kong *et al.*, Mapping of Functional Groups in Metal-Organic Frameworks. *Science* **341**, 882 (2013).
25. H. Deng *et al.*, Multiple Functional Groups of Varying Ratios in Metal-Organic Frameworks. *Science* **327**, 846 (2010).
26. J. Ilavsky, Nika: software for two-dimensional data reduction. *J. Appl. Crystallogr.* **45**, 324 (2012).
27. F. Zhang *et al.*, Glassy Carbon as an Absolute Intensity Calibration Standard for Small-Angle Scattering. *Metall. Mat. Trans. A* **41**, 1151 (2010).
28. T. Nakazono, A. R. Parent, K. Sakai, Cobalt porphyrins as homogeneous catalysts for water oxidation. *Chem. Commun.* **49**, 6325 (2013).

Acknowledgements

This research was partially supported by BASF SE (Ludwigshafen, Germany) for bulk synthesis of MOF, King Abdulaziz City of Science and Technology (Riyadh, Saudi Arabia) for MTV synthesis, and Director, Office of Science, Office of Basic Energy Sciences, Materials Sciences and Engineering Division, U.S. Department of Energy under Contract No. DE-AC02-05CH11231 for plasmonic nanocrystals. Mr. Y. Zhao is supported by the Suzhou Industrial Park fellowship. We acknowledge Mr. J. Resasco and Dr. S. Brittman for help with the ALD, Dr. K. Bustillo, Dr. H. Furukawa, and Dr. Y. Zhang for helpful discussion. This work made use of imaging, nanofabrication and inorganic facilities at the Molecular Foundry and the imaging facilities at the National Center of Electron Microscopy at Lawrence Berkeley National Laboratory and at Nanotube Research Center, AIST and at SMBU, JEOL Tokyo. Work at the Molecular Foundry is supported by the Office of Science, Office of Basic Energy Sciences, of the U.S. Department of Energy, Under Contract No.

DE-AC02-05CH11231. GIWAXS measurements were performed at the Advanced Light Source at Lawrence Berkeley National Lab. The Advanced Light Source is an Office of Science User Facility operated for the U.S. Department of Energy Office of Science by Lawrence Berkeley National Laboratory and supported by the U.S. Department of Energy under Contract No. DE-AC02-05CH11231. Z. Liu acknowledges Grant-in-Aid for Scientific Research (C) (25390023).

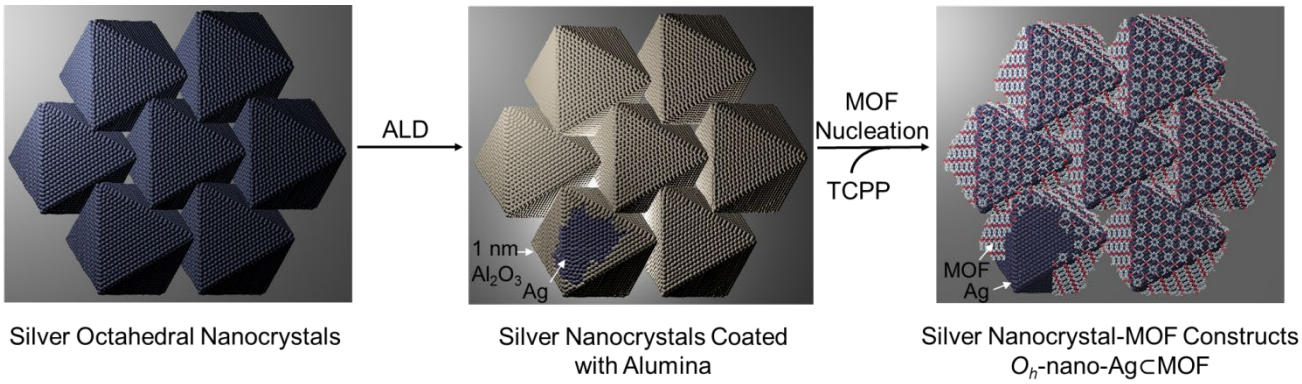

Scheme 1. The fabrication process of O_h-nano-Ag⊂MOF particles

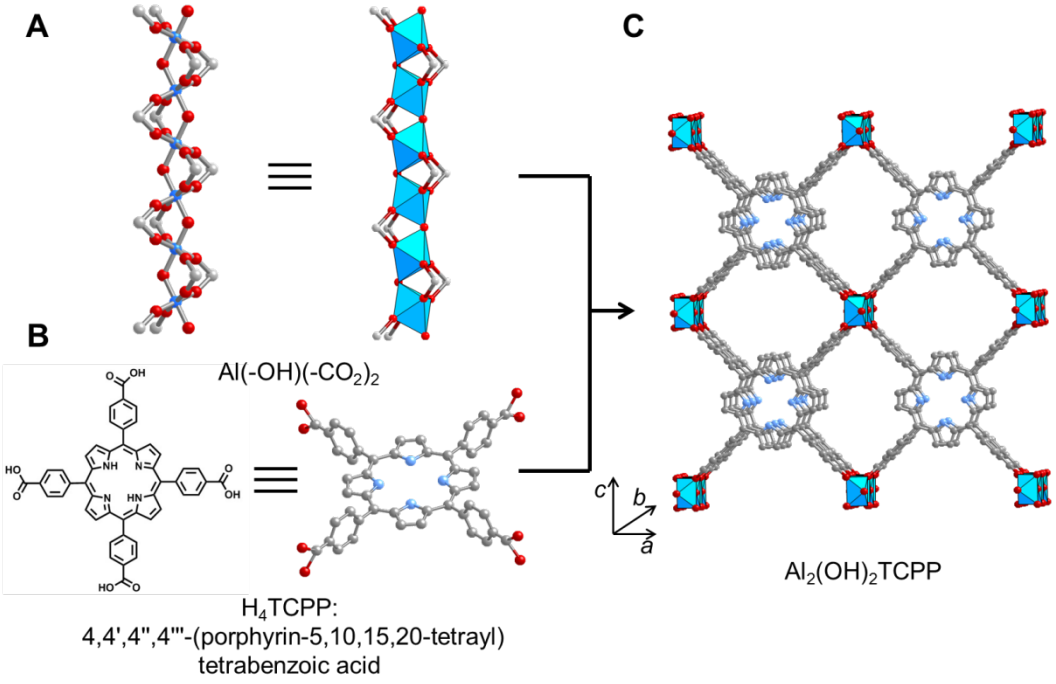

Fig. 1. The structure of $Al_2(OH)_2TCPP$ MOF. Construction of $Al_2(OH)_2TCPP$ MOF from (**A**) rod-shaped aluminum oxide units linked by (**B**) porphyrin units (H_4TCPP) to give a three-dimensional MOF (**C**) having 0.11 × 0.60 nm^2 opening along the *b*-axis . Al, blue octahedral polyhedra and blue spheres in (**A**); N, blue spheres; O, red spheres; C, gray spheres. Hydrogen atoms are omitted for clarity.

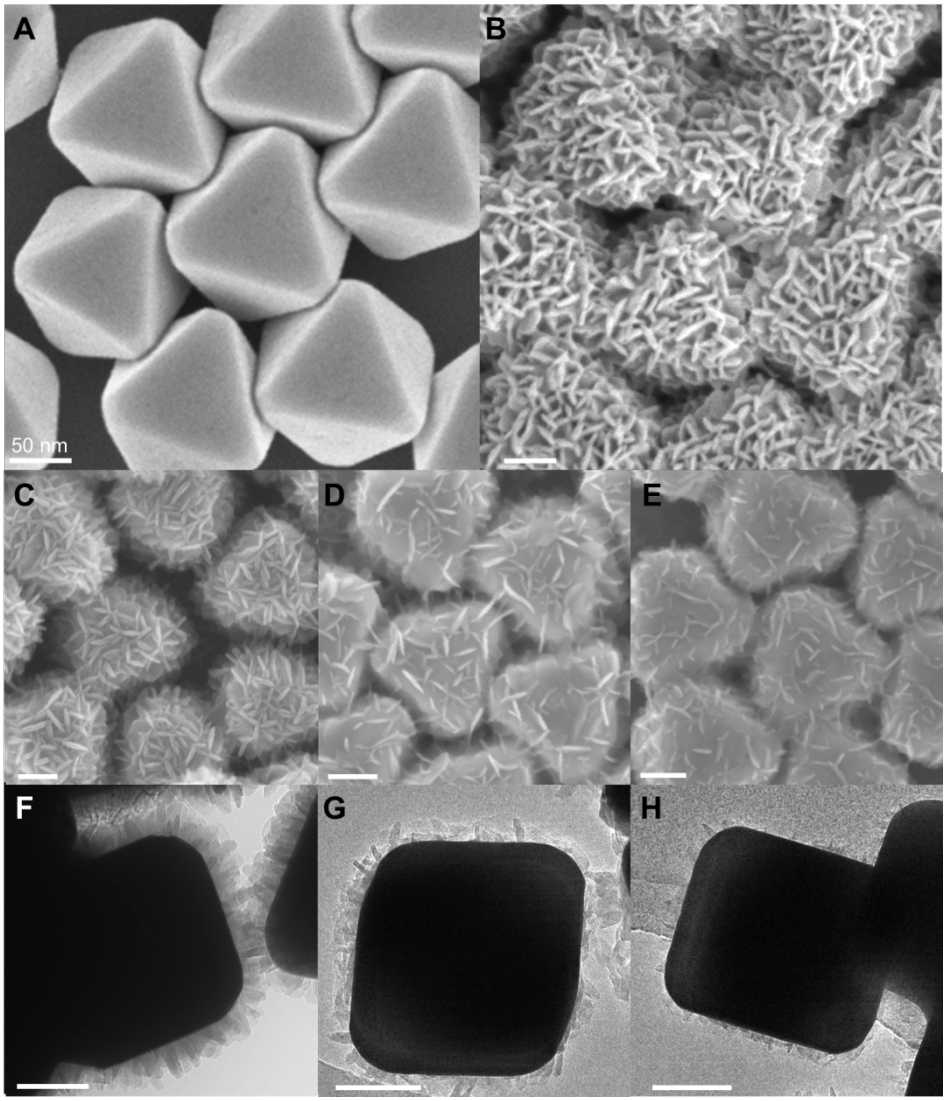

Fig. 2. The SEM and TEM images of the O_h-nano-Ag⊂MOF particles. Octahedral silver nanocrystals (**A**) are subjected to ALD deposition of alumina followed by addition of TCPP linkers to make MOF enclosed silver nanocrystals, O_h-nano-Ag⊂MOF, (**B**). Variation in the alumina thickness from 3 to 0.5 to 0.1 nm allows control of MOF coverage on the silver nanocrystals with their SEM shown

respectively (**C** to **E**) and the corresponding TEM (**F** to **H**) where the thickness and coverage of the MOF is further confirmed. The black square-like figure in **F** to **H** is the silver nanocrystal. Scale bars are all 50 nm.

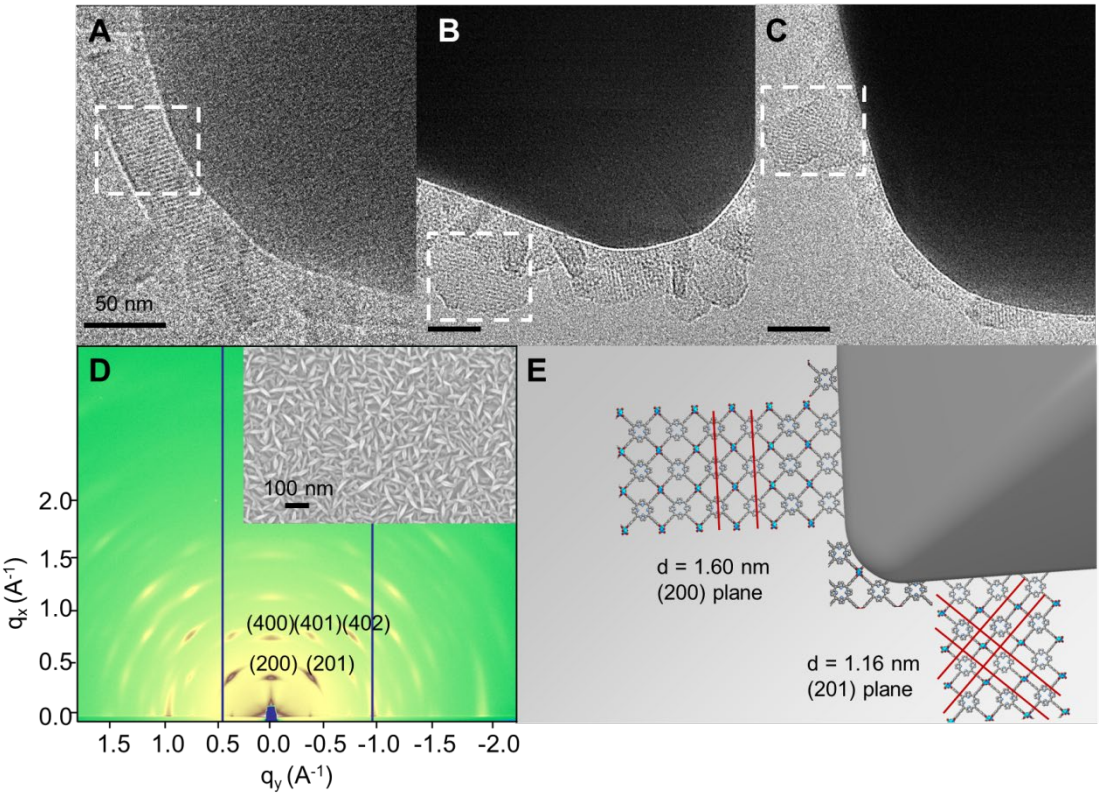

Fig. 3. Order (crystallinity) and orientation of MOF on the silver nanocrystal interface. High resolution TEM images of the O_h-nano-Ag⊂MOF showing the MOF lattice fringes of 1.16 nm (bordered by dotted rectangle) (**A**) corresponding to the MOF (201) plane, and clearly shows a pristine interface with the silver nanocrystals (large darkened shapes). Confirmation of MOF orientation is evidenced by the lattice fringes of 1.6 nm (bordered by dotted rectangle) (**B**) corresponding to the MOF (200) plane and indicating that the porphyrin units in the MOF enclosure are perpendicular to the silver nanocrystal surface. Further confirmation of this orientation is evident by the

lattice fringes of 1.16 nm (bordered by dotted rectangle) (**C**), in this case, recorded along two directions, corresponding to the (201) planes. The crystallinity of the MOF enclosure and its orientation in O_h-nano-Ag⊂MOF are confirmed by GIWAXS diffraction plot (**D**) which shows spot pattern indicative of high crystallinity and preferred orientation. The in-plane diffraction spot of MOF (200) and (400) indicates the porphyrin is perpendicular to the substrates with the *b*-axis parallel to the substrate (**D** and **E**). Another indistinguishable assignment [the in-plane diffraction spot is (001) and (002)] gives the same conclusion concerning the *b*-axis and the porphyrin orientation. The scale bars are all 20 nm.

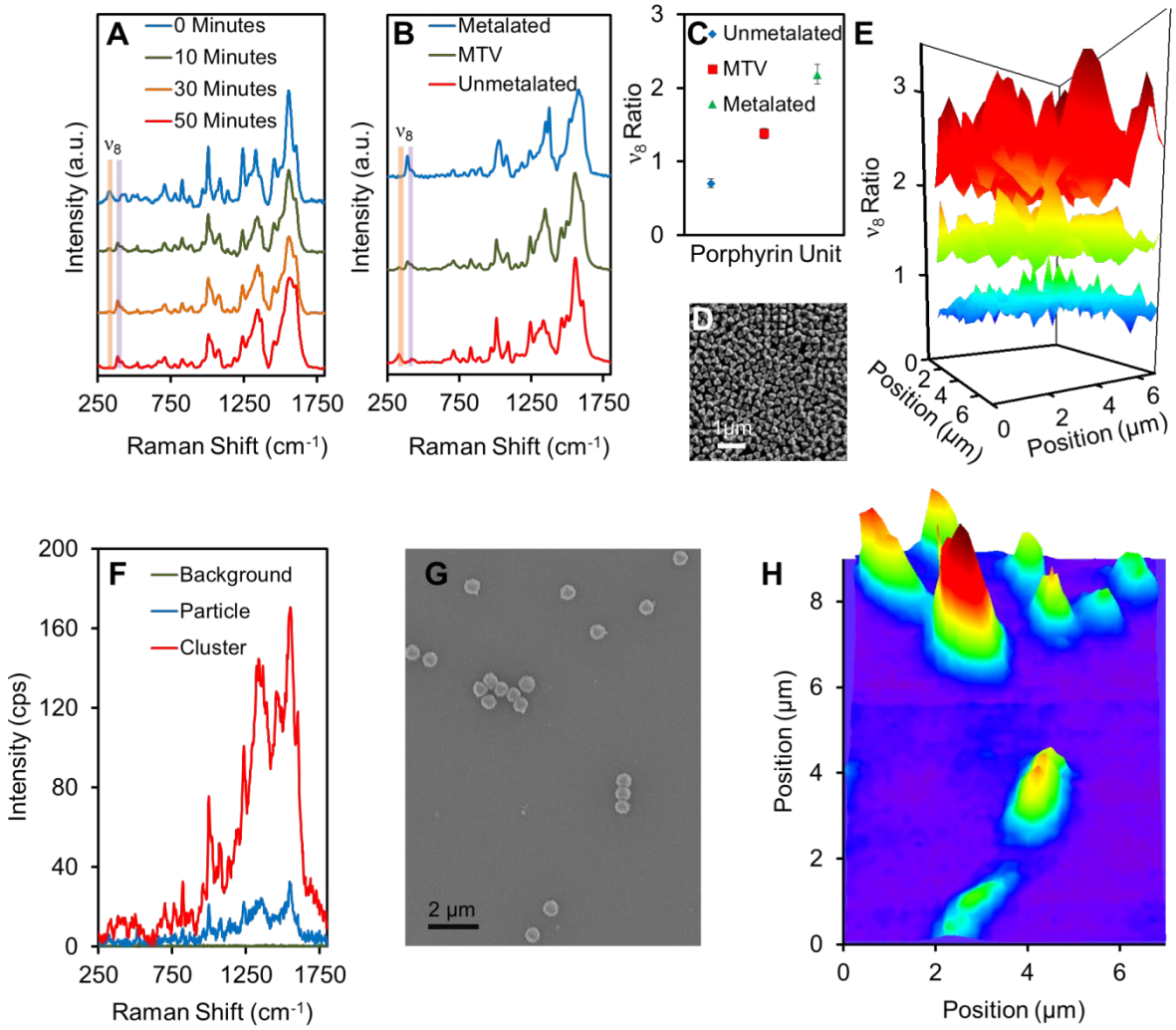

Fig. 4. Tracking metalation of MOF linkers and mapping of metalated and unmetalated linkers in O_h-nano-Ag⊂MOF using SERS. Time-dependent SERS spectroscopic tracking of metalation of the porphyrin linker units (**A**) showing the evolution of the ν_8 mode and the completion of reaction within 50 minutes. The SERS spectra for metalated, unmetalated, and multivariate metalated O_h-nano-Ag⊂MOF (B) showing the system is multivariate (MTV, mixed metalated and unmetalated MOF enclosures). The ratio of metalated and unmetalated linkers (**C**), and the homogeneity

of these in the MOF enclosures is mapped (**D**). The SERS enhancement shown for single particles and clusters of O_h-nano-Ag⊂MOF (**E**), SEM of spatially resolved discrete O_h-nano-Ag⊂MOF (**F**), and the result of their SERS mapping showing the one-to-one correspondence.